Bioorganic & Medicinal Chemistry 18 (2010) 6055–6068

Contents lists available at ScienceDirect

Bioorganic & Medicinal Chemistry

journal homepage: www.elsevier.com/locate/bmc

Synergistic experimental/computational studies on arylazoenamine derivatives that target the bovine viral diarrhea virus RNA-dependent RNA polymerase

Gabriele Giliberti [a], Cristina Ibba [a], Esther Marongiu [a], Roberta Loddo [a], Michele Tonelli [b], Vito Boido [b], Erik Laurini [c], Paola Posocco [c], Maurizio Fermeglia [c], Sabrina Pricl [c,*]

[a] Department of Biomedical Science and Technology, University of Cagliari, Cittadella Universitaria, 09042 Monserrato (Cagliari), Italy
[b] Department of Pharmaceutical Sciences, University of Genoa, Viale Benedetto XV 3, 16132 Genova, Italy
[c] Molecular Simulation Engineering (MOSE) Laboratory, Department of Chemical, Environmental, and Raw Materials Engineering, University of Trieste, Piazzale Europa 1, 34127 Trieste, Italy

ARTICLE INFO

Article history:
Received 5 January 2010
Revised 17 June 2010
Accepted 20 June 2010
Available online 25 June 2010

Keywords:
Anti-BVDV agents
Arylazoenamines
Molecular modeling
BVDV resistant mutants

ABSTRACT

Starting from a series of arylazoenamine derivatives, shown to be selectively and potently active against the bovine viral diarrhea virus (BVDV), we developed a hierarchical combined experimental/molecular modeling strategy to explore the drug leads for the BVDV RNA-dependent RNA polymerase. Accordingly, BVDV mutants resistant to lead compounds in our series were isolated, and the mutant residues on the viral molecular target, the RNA-dependent RNA polymerase, were identified. Docking procedures upon previously identified pharmacophoric constraints and actual mutational data were carried out, and the binding affinity of all active compounds for the RdRp was estimated. Given the excellent agreement between in silico and in vitro data, this procedure is currently being employed in the design a new series of more selective and potent BVDV inhibitors.

1. Introduction

Viruses belonging to the Flaviviridae family are the cause of the explosively increasing number of emerging infections of humans and economically important animals. The members of the Flaviviridae are generally classified into three genera: *Hepaciviruses*, *Flaviviruses*, and *Pestiviruses*. *Flaviviruses* are important human pathogens prevalent throughout the world, and cause a range of acute febrile illness and encephalitic and hemorrhagic diseases. Although an effective vaccine against YFV has been available since the late 1930s, utilization is incomplete in many areas.[1] Worldwide, more than 170 million people are chronically infected with the hepatitis C virus,[2–4] and thus at increased risk of developing some life-threatening liver disease (including chronic hepatitis, cirrhosis, and hepatocellular carcinoma).[5,6] The gravity of HCV infection is compounded by the inadequacy of currently approved treatments for the disease. These are based on modified interferons, and show variable success rates, due both to their limited efficacy (50–60% of patient treated) and the often associated serious side effects.[7,8] Therefore, alternative agents for the treatment and prevention of HCV infection are urgently needed.[9]

The bovine viral diarrhea virus (BVDV) is the prototype of the genus *Pestivirus* within the family of Flaviviridae. The genus *Pestivirus* contains other important animal pathogens, such as the classical swine fever virus (CSFV) and the border disease virus (BVD) that cause diseases in pigs and in sheeps, respectively.

The pathogenic biotype of BVDV in cattle causes a variety of clinical manifestations, ranging from the subclinical to death.[10–12] For the United States alone, this translates approximately into a loss of 10–40 million US$ for million calves. These losses are projected into reduced milk production, limited reproductive performance, growth retardation, and increased mortality among young stocks.[13]

To date, vaccines are available for BVDV and CSFV and massive eradication or control programs are currently implemented in many countries worldwide;[14] notwithstanding, both viruses remain a serious agronomical burden. An innovative perspective in this respect could be the prophylactic use of antiviral agents that specifically and selectively inhibit viral replications in ranches and farms in close proximity of an infected location. Herd treatment with active molecules might not only result in efficacious and rapid protection against infection but, also, in preventing virus transmission and, consequently, in avoiding massive sculling of healthy animals.

Notably, BVDV is also still considered to be a valuable surrogate virus for HCV virus.[15] Indeed, in some aspects of viral replication,

* Corresponding author. Tel.: +39 040 5583750; fax: +39 040 569823.
E-mail address: sabrina.pricl@dicamp.units.it (S. Pricl).

0968-0896/$ - see front matter © 2010 Elsevier Ltd. All rights reserved.
doi:10.1016/j.bmc.2010.06.065

BVDV is more advantageous in comparison to the currently used HCV replicon system,[16]—a surrogate cell-based system in which replication of subgenomic viral RNA can be studied—as the latter does not undergo a complete replication cycle. Hence, the early and late stages of the viral replication cycle cannot be studied in the HCV replicon system. Although very recently, robust and efficient HCV cell culture systems have been described in the literature,[17] important insight into the mechanism of antiviral activity of anti-*Pestivirus* compounds may provide valuable information for the design of novel antiviral strategies against HCV.[15,18]

The replicative cycle of all viruses of the Flaviviridae family is similar. After binding to the target receptor, the virus penetrates into the cell and its (+)-strand RNA is released from the nucleocapsid into the cytoplasm. The released viral RNA is translated into a polyprotein which, in the course of the infection, is cleaved co- and post-translationally by both host cell proteases and virus-encoded proteases. In the case of BVDV, the amino-terminal portion of the polyprotein is processed into six structural proteins (N_{pro}, C, E^{rns}, E1, E2, and p7), while the proteolitic processing of the carboxy-terminal of the polyprotein results in five mature, nonstructural proteins (NS2, NS3, NS4A, NS5A, and NS5B). Although some aspects of the mechanisms of BVDV RNA replication are still obscure, the current knowledge substantiate the evidence that BVDV employs a strategy utterly analogous to that of other (+)-strand RNA viruses. Accordingly, upon infection of cells, the genomic RNA serves as an mRNA and is translated to produce the viral nonstructural proteins which are necessary for BVDV replication. Viral RNA replication is initiated using the (+)-strand RNA as a template for the synthesis of a full length complementary minus-strand RNA. This synthesis is carried out by a membrane associated replicase complex consisting of two essential proteins of the replication cycle: the NS3 protein with its nucleoside-triphosphatase and helicase (NTPase/helicase) activities, and the NS5B, endowed with RNA-dependent RNA polymerase (RdRp) activity. The (−)-strand RNA is then transcribed into the corresponding (+)-strand RNA which, in turn, is assembled into the nucleocapsid. Importantly, both (−)- and (+)-strand viral RNA can be detected at 4 h post infection (pi), with a ratio (+)/(−) strands of 2:1 at 4 h pi, and 10:1 at 12 h pi.[19] Progeny virus can be detected as early as 8 h pi.[20] Although the NS proteins are not constituents of the virus particles, their intact functions, particularly as components of the replication complex, are essential for virus replication.[21] In this context, the NS5-associated RdRp appear to be an exceptionally attractive target for termination of viral replication.

As part of a large program of design, synthesis, in silico, and in vitro screening of new classes of non-nucleoside inhibitors of BVDV (as a surrogate for HCV), we recently reported on the activity of selected classes of arylazoenamines, 28 of which were found to elicit antiviral activity against BVDV (Scheme 1, Tables 1 and 2).[22]

Despite the high toxicity on the host cells often observed for these molecular series,[22] several compounds exhibit EC_{50} values comparable with that of the reference drug, NM-108 (EC_{50} = 1.7 μM). On the whole, the EC_{50} values for 9 of these active principles were determined to be in the sub/micromolar range (0.8–10 μM), 11 compounds had EC_{50} between 11 and 30 μM, and only 8 had EC_{50} in the range 31–100 μM.

To identify the molecular structure requirements in the available series of compounds to act as effective BVDV inhibitors, a three-dimensional pharmacophore model was also developed,[22] consisting of two hydrogen bond donor groups and one hydrophobic aromatic feature. The application of this simple but effective ligand-based approach to a test set of compounds showed that it is able to accurately predict the activity of all compounds towards the viral pathogen.

With the aim of determining whether a viral protein is targeted by our arylazoenamine series along the replication pathway of BVDV, to propose a molecular rationale for the mechanism by

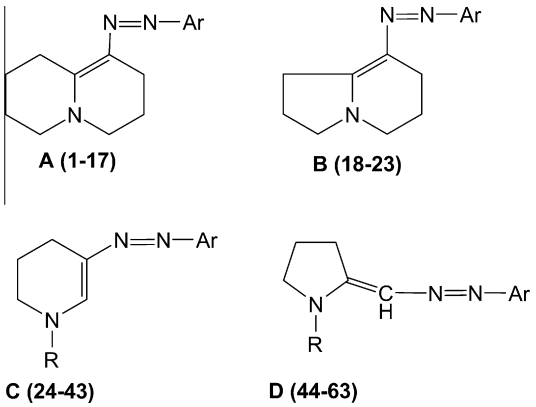

Scheme 1. Structures of the arylazoenamines considered in this work. The structural details of the entire compound series is given in Table 1.

Table 1
Antiviral activity[22] of the arylazoenamines of structure **A** (**1**–**17**) and **B** (**18**–**23**)

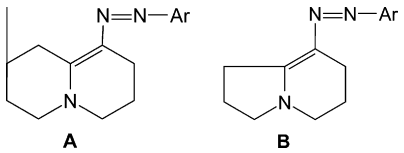

Compound	Aryl	BVDV EC_{50}[a] (μM)	Compound	Aryl	BVDV EC_{50}[a] (μM)
1	4-F-Ph	>56	**13**	3-CF_3-4-Cl-Ph	>35
2	2-Cl-Ph	>100	**14**	3-CF_3-4-Br-Ph	61
3	3-Cl-Ph	>20	**15**	3-NO_2-4-Cl-Ph	>18
4	4-Cl-Ph	>60	**16**	1-Naphtyl	6
5	3-Br-Ph	>10	**17**	7-Cl-1-quinolyl	5
6	4-Br-Ph	>59	**18**	4-Cl-Ph	>30
7	3-CF_3-Ph	>8	**19**	3-NO_2-Ph	>68
8	3-NO_2-Ph	>100	**20**	3,4-DiCl-Ph	>67
9	4-NO_2-Ph	86	**21**	3-CF_3-4-Cl-Ph	>21
10	3,4-DiCl-Ph	>30	**22**	1-Naphtyl	3.5
11	3,5-DiCF_3-Ph	>31	**23**	1-Phthalazyl	>100
12	3-CF_3-4-F-Ph	>100	NM-108 (2′-β-methylguanosine)		1.7

[a] Compound concentration (μM) required to achieve 50% protection of MDBK cells from BVDV (bovine viral diarrhea virus) induced cytopathogenicity, as determined by the MTT method.[22]

Table 2
Antiviral activity[22] of arylazoenamines of structure **C** (**24**–**43**) and **D** (**44**–**63**)

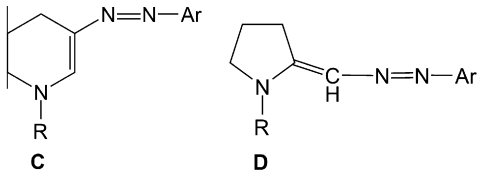

Compound	Aryl	BVDV EC_{50}[a] (μM)	Compound	Aryl	BVDV EC_{50}[a] (μM)
R = CH_3			R = CH_3		
24	Phenyl	>100	**44**	Phenyl	10
25	4-F-Ph	>48	**45**	4-F-Ph	18
26	2-Cl-Ph	100	**46**	4-Cl-Ph	21
27	3-Cl-Ph	12	**47**	3-Br-Ph	9
29	4-Cl-Ph	>58	**48**	4-Br-Ph	11
29	3-Br-Ph	19	**49**	3-CF_3-Ph	21
30	4-Br-Ph	60	**50**	3-NO_2-Ph	5.5
31	3-CF_3-Ph	90	**51**	4-NO_2-Ph	19
32	3-NO_2-Ph	0.8	**52**	4-CH_3-Ph	20
33	4-NO_2-Ph	11	**53**	4-CH_3-O-Ph	18
34	4-CH_3-Ph	>100	**54**	3,4-DiCl-Ph	16
35	3,4-DiCl-Ph	7	**55**	3,5-DiCF_3-Ph	>36
36	3,5-DiCF_3-Ph	>64	**56**	3-CF_3-4-F-Ph	100
37	3-CF_3-4-F-Ph	>100	**57**	3-CF_3-4-Br-Ph	46
38	3-CF_3-4-Cl-Ph	>28	**58**	PentaF-Ph	>100
39	3-CF_3-4-Br-Ph	40	R = CH_2–C_6H_5		
40	3-NO_2-4-Cl-Ph	>61	**59**	Phenyl	>74
41	PentaF-Ph	>100	**60**	4-Cl-Ph	>18
42	1-Naphtyl	5	**61**	4-CH_3-Ph	>22
R = CH_2–C_6H_5			**62**	3,4-DiCl-Ph	>79
43	3-CF_3-4-Cl-Ph	>28	**63**	3-CF_3-4-Cl-Ph	>14

[a] Compound concentration (μM) required to achieve 50% protection of MDBK cells from BVDV (bovine viral diarrhea virus) induced cytopathogenicity, as determined by the MTT method.[22]

which our compounds could inhibit this protein, and to develop a predictive tool for the design of a second generation of more potent and selective inhibitors, we applied a combined computational/experimental procedure which included the application of the following, sequential steps: (1) experimental isolation of BVDV mutants resistant to the most active compounds; (2) demonstration that the causal mutations resided in the NS5B, the viral RNA-dependent RNA polymerase; (3) molecular docking based upon information obtained from the 3D-pharmacophore model, and (4) molecular-mechanics/Poisson–Boltzmann/surface area (MM/PBSA) calculations to estimate the binding affinities of the compounds to the target enzyme.

2. Isolation of BVDV resistant mutants

The lead compound in our arylazoenamine derivative series, 1-methyl-3-(3-nitrophenylazo)-1,4,5,6-tetrahydropyridine (**32**), was identified as an inhibitor of BVDV replication in a multicycle growth assay (MTT assay), with an EC_{50} value of 0.8 μM and a CC_{50} >100 μM on Madin Darby Bovine Kidney (MDBK),[22] which provides a therapeutic or selectivity index (SI) higher than 125. To gain further insight on the activity of **32**, a time-of-(drug)addition experiment was performed to ascertain at what stage virus replication was inhibited by compound **32**. The kinetics of one replication cycle of BVDV was first determined by viral yield assay, as shown in Figure 1A. In agreement with previous publications,[18a,b,19,23] viral progeny was not detected until ~7 h pi, after which a considerable increase in viral yield was detected until 13 h pi Figure 1B illustrates the results from the time-of-addition experiment, during which compound **32** was added at different times pi, with progeny virus harvested at 23 h pi and quantified on MDBK cells. As can be clearly seen from Figure 1B, when **32** was added during the first 6 h pi, it resulted in the complete inhibition of virus production, with more than 10^4-fold reduction on

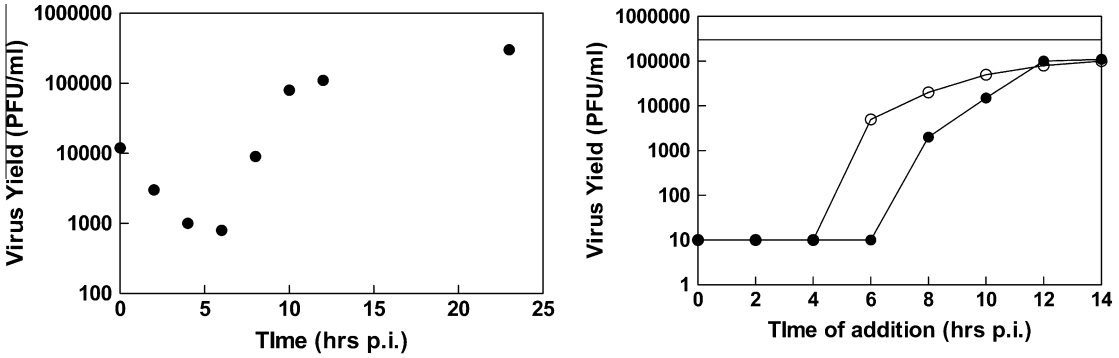

Figure 1. Effect of compound **32** on BVDV growth. (A) single cycle of BVDV replication. (B) Effect of time of drug addition on the antiviral activity of **32** (filled circles). The same test has been performed using the nucleoside analog NM-108 (open circles) for comparison. Infected control: continuous line.

viral yield observed. When **32** was added at 8 h pi, a gradual loss in its antiviral efficacy was noted. The same test was run using the reference compound NM-108 (2′-β-methylguanosine),[24] a nucleoside analog which acts as a substrate for the viral RNA-dependent RNA polymerase (RdRp), and as such incorporated into the nascent nucleic acid chain where it causes chain termination and, consequently, inhibits BVDV replication. The comparison of the two time-of-addition curves reported in Figure 1B strongly supports the indication that compound **32** is able to inhibit BVDV replication after viral entry and prior to viral budding from the infected cells. Moreover, as a single cycle of BVDV replication takes approximately 13 h on average (Fig. 1A), the gradual increase of viral yield at 6–8 h pi is very likely to coincide with the formation of functional viral replication complexes. Therefore, in keeping with previous evidences on different compounds inhibitors of the BVDV RdRp,[18,23,25] the corresponding gradual loss of antiviral efficacy of **32** noted at a time point later than 6 h pi corroborates the hypothesis that it may act as an allosteric inhibitor of the viral polymerase as well.

In a further effort to confirm the molecular target underlying the viral activity of our compound series, compound-**32**- and compound-**42**-resistant viruses were selected. Beside indications on the molecular target, the isolation of BVDV resistant strains and the determination of the causal mutations involved in drug resistance would constitute fundamental information for driving the successive molecular docking operation.

32^R and **42**^{R} BVDV viruses were selected propagating wild-type BVDV in MDBK cells in the presence of increasing concentrations of the antiviral agents. To determine the gene targeted by our compounds, the region of the BVDV genome encoding the non structural proteins NS3-NS5B was sequenced. By comparing the sequences of this region obtained from the **32**^{R} and **42**^{R} clones to the parent wild type strains (GeneBank Accession number AJ781045), mutations were detected at three different positions of the NS5B, that is, the gene that encodes the RdRp. No other mutations were found throughout the NS region of the drug-resistant virus genes. These positions, together with the corresponding wild-type/mutated residues and the concentrations at which drug-resistant viruses were isolated, are summarized in Table 3.

Interestingly, both **32**^{R} and **42**^{R} BVDV clones feature a change in the amino acid coding sequence from a glutamic acid to a glycine at position 291 along the primary sequence of the RdRp. This mutation has already been demonstrated to be sufficient and necessary to confer resistance to compound-1453, a cyclic urea derivative inhibitor of the BVDV RNA-dependent RNA replicase,[18a] and AG110, an imidazopyrrolopyridine that potently prevents the *Pestivirus* replication.[18f] Mutation I261 M identified in the **42**^{R} virus was recently reported by us to be involved in BVDV resistance against some potent and selective 2-phenylbenzimidazole derivatives,[26] whilst the other mutation, K131E, found in the **32**^{R} clone, has not been reported so far. Finally, the mutation S176R, present in both resistant isolates, is likely not to be involved in drug resistance, as there are several wild type strains of BVDV having an arginine at position 176.

The important residues found mutated in the isolated drug-resistant BVDVs—E291G, I261 M, and K131E—are located in the finger domain of the RdRp (vide infra). This region, in analogy with structurally-related HCV RdRp, is believed to play several critical roles in the enzyme activity, ranging from modulation of finger flexibility for template/product translocation, eventual dimerization of the RdRp in the replication complex, or protein–protein interactions, enabling the assembly of an active replication complex.[27] Also, quite interestingly, these amino acids locate in the close vicinity of F224, a residue previously reported as mutated in BVDV viruses resistant to other highly selective inhibitors, for example, (3-[((2-dipropylamino)ethyl)thio]-5*H*-1,2,4-triazino[5,6-*b*]indole (VP32947)[23] and 5-[(4-bromophenyl)methyl]2-phenyl-5*H*-imidazo[4,5-*c*]pyridine (BPIP).[18b]

Noticeably, **32**^{R} virus was found fully resistant not only to compound **42**, as expected, but also to three potent BVDV inhibitors based on a benzimidazole scaffold used as test molecules, as shown in Table 4.

The overall results reported above clearly support the hypothesis that not only the BVDV RNA-dependent RNA polymerase is the protein target for our arylazoenamine derivatives, but also that the E291G mutation in this viral protein in particular is responsible for the viral phenotypes resistant against this molecular series. To examine this inhibition in more detail, we cloned and expressed the BVDV NS5B,[28] and studied the effects of compounds **32** and **42** on the activity of this viral protein. The enzymatic inhibition assays showed that these compounds inhibit the RNA polymerase at micromolar concentrations, in a dose dependent way, ultimately indicating that the RdRp is indeed their target. Since BVDV is often used as a surrogate model to screen antiviral agents against HCV, the two compounds were also assayed against HCV1b polymerase and found to inhibit this enzyme with similar IC_{50} values, as shown in Table 5.

3. Molecular docking onto the BVDV RdRp

The crystal structure of RdRp from several families of single- or double-strand RNA viruses, including BVDV,[29,30] have been recently made available in the Protein Data Bank (PDB) repository. As other RdRps, the tertiary structure of this protein from BVDV presents the shape of a right hand, composed by fingers, palm, and thumb domains. In particular, the BVDV RNA-dependent RNA polymerase core domain (residues 139–679) has dimensions of approximately 74 × 60 × 58 Å around a central cavity,[29] which serves for RNA template binding, nucleotides recruitment, and polymerization reaction. In addition, there is an N-terminal region

Table 4
Susceptibility of wild type and **32**^{R} BVDV to compound **42** and three benzimidazole derivatives[26]

Compound	CC_{50} (μM) MDBK	EC_{50} (μM) $BVDV^{wt}$	EC_{50} (μM) **32**^{R}
42	>100	5	>100
C1[a]	>100	0.8	>100
C2[a]	58	1	>100
C3[a]	79	1.5	>79

[a] These compounds have the general formula 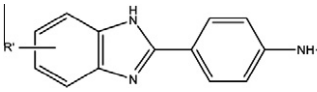 where: R′ = 5-NO_2 and R‴ = CH_3CO for **C1**, R′ = 5,6-diCl and R‴ = CH_3CO for **C2**, and R′ = 5-NO_2 and R‴ = H for **C3**, respectively.

Table 3
Mutated residues in **32**^{R} and **42**^{R} BVDV RNA dependent RNA polymerase (NB5B RdRp), and relevant concentrations at which the resistant viruses were isolated

Compound	× EC_{50} (μM)	Mutations
32	16	K131E, S176R, E291G
42	16	S176R, I261M, E291G

Table 5
In vitro BVDV and HCV1b polymerase inhibition assay for compounds **32** and **42**

Compound	IC_{50} (μM) BVDV	IC_{50} (μM) HCV
32	32	30
42	28	55

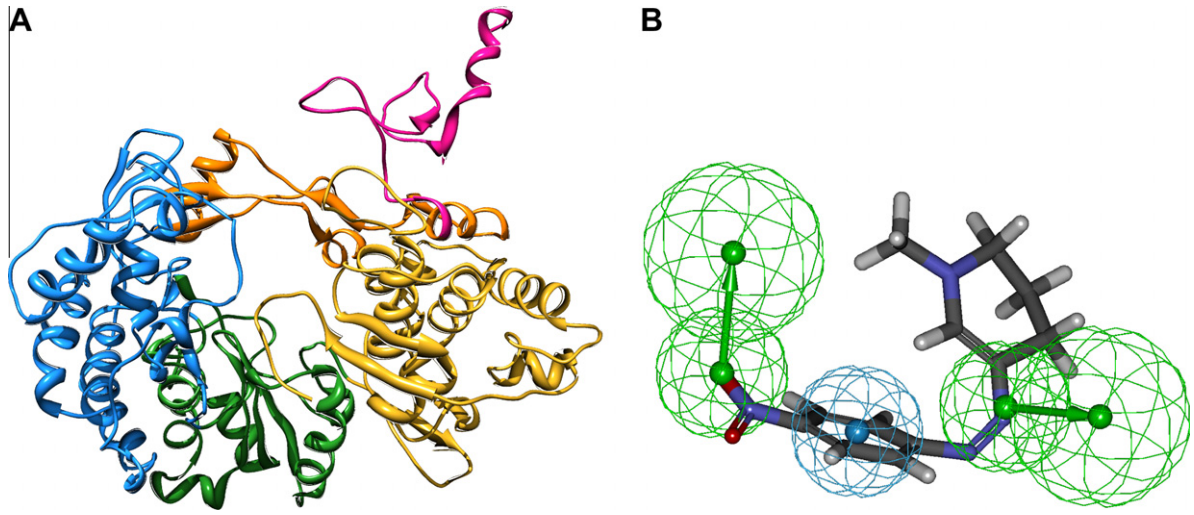

Figure 2. (A) Overview of the entire structure of the RdRp of BVDV. The protein domains are colored as follows: hot pink, N-terminal domain (residues 93–138); dodger blue, finger domain (residues 139–313 and 351–410); palm domain, forest green (residues 314–350 and 411–500); golden rod, thumb domain (residues 501–679). The N-terminus of the finger domain which, together with a long insert in the fingers domain forms the fingertip region (residues 137–173 and 260–288) is highlighted in orange. (B) Mapping of the most active compound **32** onto the 3D pharmacophore model developed for this series of compounds.[22] The hypothesis features are portrayed as mashed spheres, color-coded as follows: light blue, hydrophobic aromatic (HYAr); light green, hydrogen bond acceptor (HBA). The HBA feature is actually represented as a pair of spheres (the smaller sphere represents the location of the HBA atom on the ligand and the larger one the location of an HB donor on the receptor).

(residues 71–138) of which residues 71–91 are disordered in the relevant crystal structure (see Fig. 2A).

In a previous work, we employed a ligand-based computational approach to identify the molecular structure requirements in the present series of compounds to act as effective BVDV inhibitors.[22] The highly predictive three-dimensional pharmacophore model generated consisted of two hydrogen bond donor and one hydrophobic aromatic feature, as illustrated in Figure 2B. Using these constraints combined with the information on key amino acids identified by mutation (see Section 2), we searched for a putative binding site of our molecular series on BVDV RdRp, following our recently published successful protocol developed for studying allosteric inhibitors of BVDV,[26,31] and Polio-virus helicase.[32] In line with previous findings, the resulting portion of the enzyme making up the putative binding site interacting with the inhibitors is located in the fingers domain (residues 139–313 and 351–410), consisting of 12 α-helices and 11 β-strands (see Fig. 3). In BVDV RdRp, as in other viral RdRps, the N terminus of the fingers domain, together with a long insert in the fingers domain (residues 260–288), form the fingertip region that associates with the thumb domain. This region is characterized by a three-strand conformation, and since the fingers and the thumb domains are associated through this fingertip region, the conformational change induced by the RNA template binding into the central channel is somewhat limited. The remainder of the fingers domain is comprised of a β-strand rich region (β-fingers) and a α-helix rich region (α-fingers) close to the palm domain. The fingertip region contains polymerase motifs I and II, which are involved in RNA template and NTP binding. Mutagenesis studies in this region of this protein (and on the analogous enzyme from HCV) have been shown to result in drastically reduced polymerase activity.[34] Thus, the fingertip region seems to play a major role in the polymerase working mechanism, and it could seem conceivable that the flexibility of the fingertip region is an intrinsic property of the polymerase, necessary for binding and translocation of template during the nascent strand elongation process.

According to the procedure adopted, all compounds were characterized by a similar docking mode in the putative binding site of the BVDV RdRp, as exemplified by compound **32** in Figure 3.

An analysis of the best docking pose of **32** into the putative binding site of BVDV RdRp reveals that three residues lining the pocket are found to satisfy the pharmacophore hypothesis requirements (see Fig. 3D). The first hydrogen bond acceptor (HBA) feature on the inhibitor, represented by an oxygen atom of the nitro group (see Fig. 2B), localizes hydrogen bond acceptor structures that are in an ideal position for forming hydrogen bonds with the donor guanidinium group of R295 on the receptor. The second HBA feature of **32**, represented by one of the nitrogen atoms of the aza group (see Fig. 2B), finds its counterpart in the terminal NH_2 group of N217. The remaining hydrophobic aromatic feature (HYAr) is satisfied both by a partial π–π stacking interaction of the aromatic rings of **32** and the side chain of Y674 in an edge-on (T-stacking) geometry, and an apt encasement of the phenyl ring of the inhibitor in an extended hydrophobic cage (see Section 4 for a detailed discussion). Finally, the amino acids found mutated in BVDV RdRp variants resistant to our series of compounds (Table 3 and Fig. 3D) are also located in close distance to the inhibitor, and this evidence could ultimately account for the inactivity of these series against viruses expressing these mutated proteins.

4. MM/PBSA drug/protein affinity calculations

The ability to accurately predict binding affinities from structural considerations is an essential prerequisite to develop a thermodynamically sound strategy for drug design. Further, the quests for computationally expeditious yet reliable methods for obtaining free energy of binding estimates for a considerable number of compounds to a given receptor is still a critical issue to be used along the process of structure-based drug design.[35,36]

Despite the enormous size of the conformational space for a given ligand, current docking methodologies have been successfully employed by our group in reproducing crystallographic evidences as well as to predict putative binding modes.[22,28,31,32,37] However, conformational sampling also plays an important role in calculating the binding free energy accurately and efficiently. The conformational flexibility of a given inhibitor and its receptor can be taken into account, resorting to a wise strategy that employs a rapid and lower level method such as flexible inhibitor/rigid receptor docking at the beginning (Section 3), and turning to the more accurate and quantitative method as the MM/PBSA analysis[35] sampled by molecular dynamics (MD) simulations only once the best

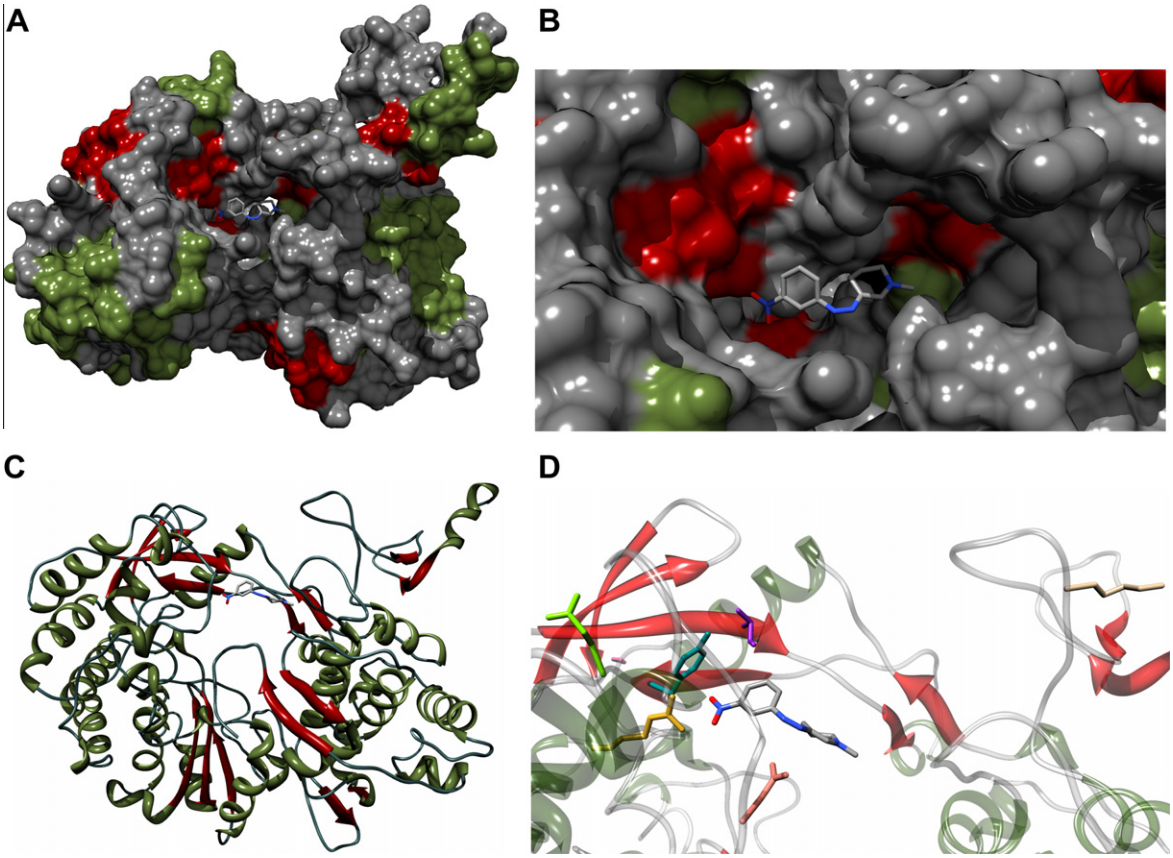

Figure 3. (A) Overall and (B) detailed space filling representation of the BVDV RdRp molecular surface and compound **32** docked into the protein putative binding site. The inhibitor is in a stick representation, with carbons in gray, nitrogens in blue, and oxygens in red. (C) Ribbon diagram of BVDV RdRp/**32** complex structure as resulting from the applied docking procedure. The protein is colored according to its secondary structure: α-helices, dark olive green; β-sheets, dark red; coils, dark slate gray. The inhibitor **32** is again in stick representation (color code as above). (D) Details of compound **32** in the binding pocket in the enzyme fingertip motif. Color scheme as above. The side chains of the three residues satisfying the 3D pharmacophore model requirements for the interaction with compound **32**, and those of the residues involved in resistant mutations, are shown as colored stick models, according to the following color-coding: K131, tan; S176, hot pink; N217, salmon; I261, purple; Y289, dark cyan; E291, chartreuse; R295, golden rod. Hydrogen atoms, counterions, and water molecules are omitted for clarity.

pose has been identified and all eventual available criteria have been satisfied.

According to this computational perspective, we performed MM/PBSA calculations for the 28 compounds endowed with activity against BVDV, starting from the corresponding BVDV RdRp/inhibitor complex structures obtained from the docking procedure described in the preceding section. In MM/PBSA calculations, the affinity of a ligand binding to a protein can be estimated by two protocols: (i) evaluate all terms using separate trajectories of complex, protein, and ligand (separate-trajectory protocol) or (ii) using the snapshots from the MD trajectory of the complex (single-trajectory protocol). Indeed, pathway (ii) is much faster than (i) and potentially requires less sampling because of the intramolecular energies cancel out when calculating the association energy. Upon comparing results obtained from using both protocols on some tests compounds and the influence of different length of conformational sampling (data not shown), and considering the high stability of the prediction, the single-trajectory protocol was then applied throughout this study.

The calculated ΔG_{bind} values for all molecules are listed in Table 6.

According to the energy components of the binding free energies ΔG_{bind} (Table 6), the major favorable contributions to ligand bindings are van der Waals (ΔE_{VDW}) and electrostatic (ΔE_{EL}) terms, whereas polar solvation (ΔG_{PB}) and entropy ($T\Delta S$) terms oppose binding. Nonpolar solvation terms (ΔG_{NP}), which correspond to the burial of the solvent-accessible surface area (SASA) upon binding, contribute slightly favorably. Specifically, for this series of compounds, the mean value of the electrostatic energy ($\Delta E_{EL} + \Delta G_{PB}$) is approximately +32 kcal/mol, whilst the corresponding mean values of the van der Waals and hydrophobic overall interaction energies ($\Delta E_{VDW} + \Delta G_{NP}$) are −53 kcal/mol, confirming that, in line with several previous findings, the association between the ligands and the RdRp is mainly driven by more favorable nonpolar interactions in the complex than in the solution, in keeping with a proposed general scheme for non-covalent associations.[22,28,31,32,37,38] The calculated changes in solute entropy, $-T\Delta S$, are physically reasonable and confined within a small range of values, an expected results as the major role in determining the overall conformation of these compounds is played by the invariant presence of the rigid aza moiety bound to the aromatic ring. More importantly, it is quite encouraging that the experimental rank of our compound series toward BDVD RdRp is well consistent with our in silico prediction (vide infra for a detailed discussion).

The application of the MM/PBSA analysis on the lead compound **32** reveals further, interesting details about the binding modes of this compound with the residues lining the putative binding site on the surface of the BVDV RdRp (see Fig. 4A). In particular, the nitro group of the inhibitor is able to establish a bifurcated hydrogen bond with the guanidinium group of R295, characterized by a dynamic average length (ADL) of 2.6 ± 0.1 Å and 2.9 ± 0.2 Å, respectively, as evidenced in Figure 4B. This interaction satisfies the first 3D pharmacophore requirement, that is, the HBA feature. Further, one nitrogen atom of the aza moiety present on the inhibitor is

Table 6
Free energy components and total binding free energies for the 28 arylazoenamine compounds active on BVDV RdRp

	9	**14**	**16**	**17**	**22**	**26**	**27**	**29**	**30**	**31**	**32**
ΔE_{VDW}	−45.26 (0.14)	−46.51 (0.12)	−49.24 (0.13)	−49.72 (0.13)	−48.83 (0.15)	−47.79 (0.16)	−49.03 (0.12)	−49.32 (0.16)	−47.76 (0.15)	−46.92 (0.13)	−49.02 (0.11)
ΔE_{EL}	−23.72 (0.25)	−21.95 (0.24)	−22.19 (0.24)	−21.88 (0.27)	−23.35 (0.25)	−23.01 (0.27)	−22.49 (0.24)	−22.36 (0.26)	−22.03 (0.28)	−22.99 (0.30)	−23.65 (0.23)
ΔG_{PB}	55.42 (0.22)	54.92 (0.19)	55.25 (0.21)	54.98 (0.19)	53.37 (0.23)	54.03 (0.24)	55.56 (0.19)	56.03 (0.21)	55.98 (0.22)	53.43 (0.23)	53.98 (0.19)
ΔG_{NP}	−4.75 (0.00)	−5.43 (0.01)	−5.07 (0.01)	−5.15 (0.01)	−4.99 (0.00)	−4.15 (0.01)	−5.01 (0.01)	−5.30 (0.00)	−5.61 (0.01)	−5.32 (0.00)	−5.27 (0.00)
$T\Delta S_{solute}$	11.28 (0.83)	11.76 (0.86)	12.65 (0.83)	13.02 (0.75)	14.91 (0.80)	13.99 (0.89)	12.74 (0.95)	12.98 (0.75)	12.20 (0.91)	14.74 (0.98)	14.17 (0.72)
ΔG_{bind}	***−7.03***	***−7.21***	***−8.60***	***−8.75***	***−8.89***	***−6.93***	***−8.23***	***−7.97***	***−7.22***	***−7.06***	***−9.79***
	33	**35**	**39**	**42**	**44**	**45**	**46**	**47**	**48**	**49**	**50**
ΔE_{VDW}	−49.94 (0.12)	−47.93 (0.12)	−48.17 (0.15)	−49.83 (0.14)	−49.75 (0.15)	−48.78 (0.16)	−48.16 (0.13)	−49.22 (0.15)	−49.75 (0.11)	−47.37 (0.12)	−49.78 (0.14)
ΔE_{EL}	−22.37 (0.26)	−24.60 (0.30)	−22.03 (0.26)	−23.02 (0.24)	−23.11 (0.25)	−21.45 (0.28)	−23.31 (0.29)	−25.06 (0.28)	−23.74 (0.25)	−24.01 (0.28)	−23.72 (0.26)
ΔG_{PB}	56.01 (0.21)	55.89 (0.20)	56.22 (0.23)	56.02 (0.21)	57.10 (0.23)	54.97 (0.18)	54.59 (0.21)	57.82 (0.21)	58.23 (0.24)	53.89 (0.23)	55.56 (0.20)
ΔG_{NP}	−4.89 (0.01)	−5.73 (0.00)	−4.78 (0.01)	−5.36 (0.01)	−4.48 (0.01)	−5.22 (0.00)	−4.43 (0.00)	−4.99 (0.01)	−4.36 (0.01)	−5.02 (0.01)	−4.32 (0.01)
$T\Delta S_{solute}$	12.93 (0.83)	13.82 (0.92)	11.30 (0.77)	13.41 (0.82)	12.15 (0.85)	12.53 (0.93)	13.23 (0.87)	13.09 (0.86)	11.38 (0.73)	14.63 (0.91)	13.63 (0.81)
ΔG_{bind}	***−8.26***	***−8.55***	***−7.46***	***−8.78***	***−8.29***	***−7.95***	***−7.87***	***−8.36***	***−8.24***	***−7.88***	***−8.63***
	51	**52**	**53**	**54**	**56**	**57**					
ΔE_{VDW}	−48.63 (0.13)	−45.93 (0.11)	−50.07 (0.14)	−43.69 (0.16)	−47.53 (0.14)	−46.72 (0.11)					
ΔE_{EL}	− 21.53 (0.25)	−21.32 (0.30)	−21.47 (0.24)	−20.44 (0.25)	−19.15 (0.24)	−21.04 (0.29)					
ΔG_{PB}	55.18 (0.19)	53.34 (0.25)	54.82 (0.20)	47.95 (0.18)	50.61 (0.23)	52.15 (0.20)					
ΔG_{NP}	−5.60 (0.01)	−5.97 (0.00)	−4.81 (0.00)	−6.02 (0.01)	−4.88 (0.01)	−4.26 (0.00)					
$T\Delta S_{solute}$	12.67 (0.97)	11.99 (0.70)	13.55 (0.79)	14.12 (0.98)	14.01 (0.89)	12.37 (0.93)					
ΔG_{bind}	***−7.91***	***−7.89***	***−7.98***	***−8.08***	***−6.94***	***−7.47***					

All values are in kcal/mol. Errors are given in parenthesis as standard errors of the mean.

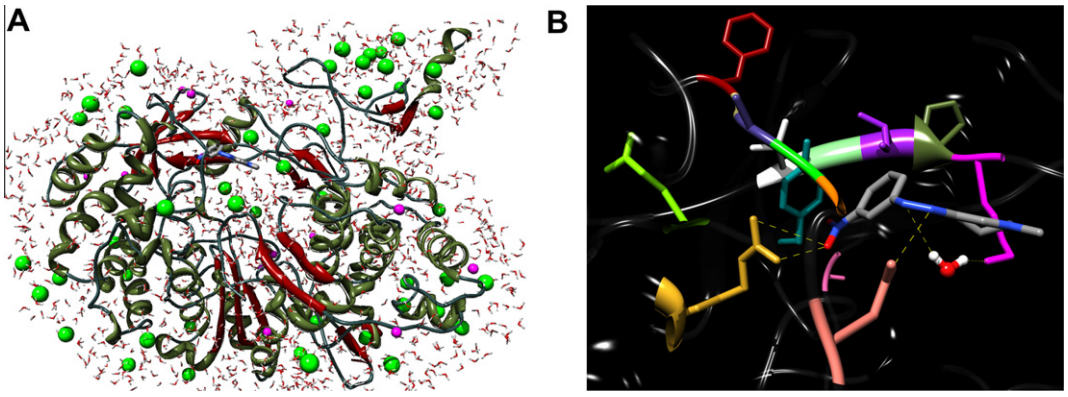

Figure 4. (A) Ribbon diagram of BVDV RdRp/**32** complex structure taken from an equilibrated molecular dynamics snapshot. The protein is colored according to its secondary structure: dark olive green, α-helices; dark red, β-strands, dark slate gray, coils. The inhibitor **32** is represented as a stick model with carbons in gray, nitrogens in blue, and oxygens in red (hydrogens are not shown). A shell of water molecules is depicted as atom-colored lines. Chlorine and sodium counterions are visualized as green and magenta spheres, respectively. (Note that spheres and sticks size are not in scale for graphical purposes). (B) Details of compound **32** (in a stick representation) in the binding pocket in the enzyme fingers domain. Hydrogen bonds are highlighted as light yellow broken lines. The water molecule engaged in hydrogen bonding is portrayed as atom-colored sticks-and-balls (red, oxygens, white, hydrogens). The side chains of all residues that form the primary binding pocket interacting with **32**, including the mutant residues are shown as stick models, and the color coding is the following: S176, hot pink; N217, salmon; G220, orange; A221, green; A222, dark slate blue; G223, dark kaki; F224, dark red; T259, white; A260, light green; I261, purple; P262, dark olive green; K263, magenta; Y289, dark cyan; E291, chartreuse; R295, golden rod. Residue K131 is out of sight.

found to be engaged in stable hydrogen bond with the NH_2 group of the side chain of N217, with ADL = 3.1 ± 0.2 Å, thus fulfilling the second HBA pharmacophore feature. Finally, the aromatic ring of **32** is nicely encased in a hydrophobic subsite, delimited by the backbone and side chains of the ceiling residues T259, A260, I261, on one side and P262 on one side, and G220, A221, A222, and G223 on the other. Also, the phenyl ring is further stabilized by favorable dispersion forces due to a partial π–π stacking with Y289. Accordingly, the third pharmacophore feature (i.e., HYAr) is also completed by this plethora of hydrophobic interactions.

Finally, the second nitrogen atom of the –N=N– group is also engaged in a persistent, water-mediated hydrogen bond (through water 1522) with the side chain $-NH_3^+$ moiety of K263 (ADL = 2.9 ± 0.2 Å and 3.0 ± 0.1 Å, respectively, see Figure 4B). The presence of all these stabilizing interactions account for the favorable value of the estimated free energy of binding (ΔG_{bind} = −9.79 kcal/mol, EC_{50} = 0.8 μM), for this inhibitor of the BVDV RdRp, making it the lead compound for this molecular series.

Compound **27** shows an intermediate affinity for the BVDV polymerase target, being characterized by an estimated ΔG_{bind} = −8.23 kcal/mol, and an experimental EC_{50} value of 12 μM. The analysis of the corresponding MD trajectory reveals that this compound is missing one of the critical H-bond, required for optimal pharmacophore mapping (see Fig. 5A). Nevertheless, all other stabilizing interactions, including the hydrogen bond between the first N atom of the –N=N– group and N217 (ADL = 2.9 ± 0.2) and the water-mediated hydrogen bond between the nitrogen of the aza moiety and the side chain of K263 (ADL = 3.1 ± 0.1 Å and 3.2 ± 0.1 Å, respectively), are persistently detected along the entire 10 ns trajectory, thus accounting for the corresponding inhibitory capacity of this compounds with respect of its viral target receptor.

Finally, it is instructive to consider the MD evidences for **56**, one of the least active compounds (ΔG_{bind} = −6.94 kcal/mol, EC_{50} = 100 μM). The analysis of the MD trajectory reveals only the existence of an intermittent, short lived H-bond bridging the –N=N– group to the side chain of K263 via water 2156. However, as exemplified in Figure 5B, along the entire MD run this molecule is not able to adjust its conformation within the putative binding site of the receptor so as to fulfill the intermolecular interaction required for a productive binding. Accordingly, only a very low activity, if at all, is predicted, in accordance with both in silico and experimental data.

In order to gain a deeper insight of the binding energetics and mechanism of our compound series, we split the total free energy of RdRp binding into contributions from individual ligand–residue pairs, as shown in Figure 6 for compounds **32**, **27** and **56** as representative examples. In accordance with the visual inspections and the geometrical evidences reported in Figures 4 and 5, four major clusters centering around the key residues S176, N217, I261, and R295 emerged. Of note, all these important residues are involved in strong van der Waals interactions and/or topical hydrogen bonding with the inhibitors. A further observation stemming from this energy decomposition analysis is that, in line with the corresponding EC_{50} and ΔG_{bind} values, the overall number and the intensity of these interactions correctly decrease in the order **32** > **27** ≫ **56**. This, in turn, results in comparable van der Waals contacts between **32** and **27** (i.e., ΔE_{VDW} = −49.02 and −49.03 kcal/mol, respectively, see Table 6), and in a neat decrease for the same quantity in the case of compound **56** (−47.53 kcal/mol). Concomitantly, this is reflected in the opposite behavior of the electrostatic contribution to binding, where the progressive disappearance of pharmacophore-required H-bonds leads to a substantial loss of stabilizing interactions for the three compounds in the correct order (i.e., ΔE_{EL} = −23.65, −22.49, and −19.15 kcal/mol for **32**, **27**, and **56**, respectively, see Table 6).

Ideally, during in silico lead-discovery study, the applied computational recipe should be able to estimate the activity of new compounds prior to their synthesis. To verify if our MM/PBSA approach could be useful to this purpose, we classified our set of compounds on the basis of their activity as moderately active ($EC_{50} \leq 15$ μM, +++), weakly active ($15 < EC_{50} < 100$ μM, ++), and inactive ($EC_{50} \geq 100$ μM, +). Then, according to this classification and taking into account the ΔG_{bind} values listed in Table 6, we can easily see that, among the 28 molecules, all 13 active principles having a ΔG_{bind} value larger than or equal to −8 kcal/mol can be classified as active (+++), the 13 moderately active inhibitors characterized by -8 kcal/mol $< \Delta G_{bind} \leq -7$ kcal/mol are ranked properly (++), and the 2 inactive compounds with ΔG_{bind} smaller than −6 kcal/mol are correctly classified as such (+).

A further step in our modeling procedure consisted of modeling the two lead compounds for which resistant mutant proteins were identified (i.e., **32** and **42**) in the corresponding BVDV RdRp binding site (see Fig. S1) and to estimate the relevant binding energies. This, with the ultimate goal of testing the ability of the current computational methodology to account for observed drug resistance (see Section 2). Table 7 reports the calculated free energy of binding values and their components for **32** and **42** in complex with K131E/E291G and I261M/E291G mutant BVDV RdRps, respectively.

It is quite encouraging to see that the estimated values of the affinities for the two compounds **32** and **42** with respect to the corresponding resistant mutant RdRp isoforms are in line with the

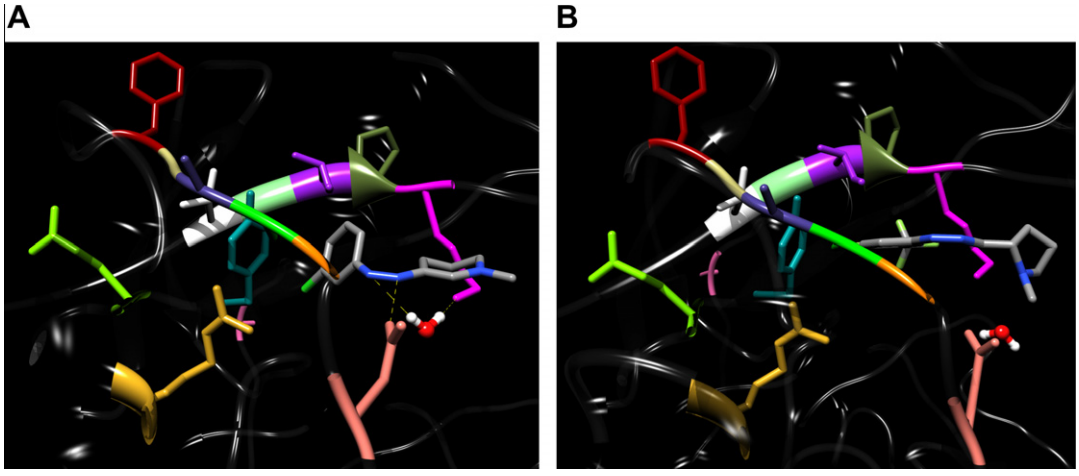

Figure 5. Zoomed view of compounds **27** (A) and **56** (B) in the binding pocket in the enzyme fingers domain. The inhibitor is represented as a stick model with carbons in gray, nitrogens in blue, and oxygens in red (hydrogens are not shown). Hydrogen bonds are highlighted as light yellow broken lines. The water molecule engaged in hydrogen bonding is portrayed as atom-colored sticks-and-balls (red, oxygens, white, hydrogens). The side chains of all residues that form the primary binding pocket interacting with **32**, including the mutant residues are shown as stick models, and the color coding is the following: S176, hot pink; N217, salmon; G220, orange; A221, green; A222, dark slate blue; G223, dark kaki; F224, dark red; T259, white; A260, light green; I261, purple; P262, dark olive green; K263, magenta; Y289, dark cyan; E291, chartreuse; R295, golden rod. Residue K131 is out of sight, as in Figure 4B.

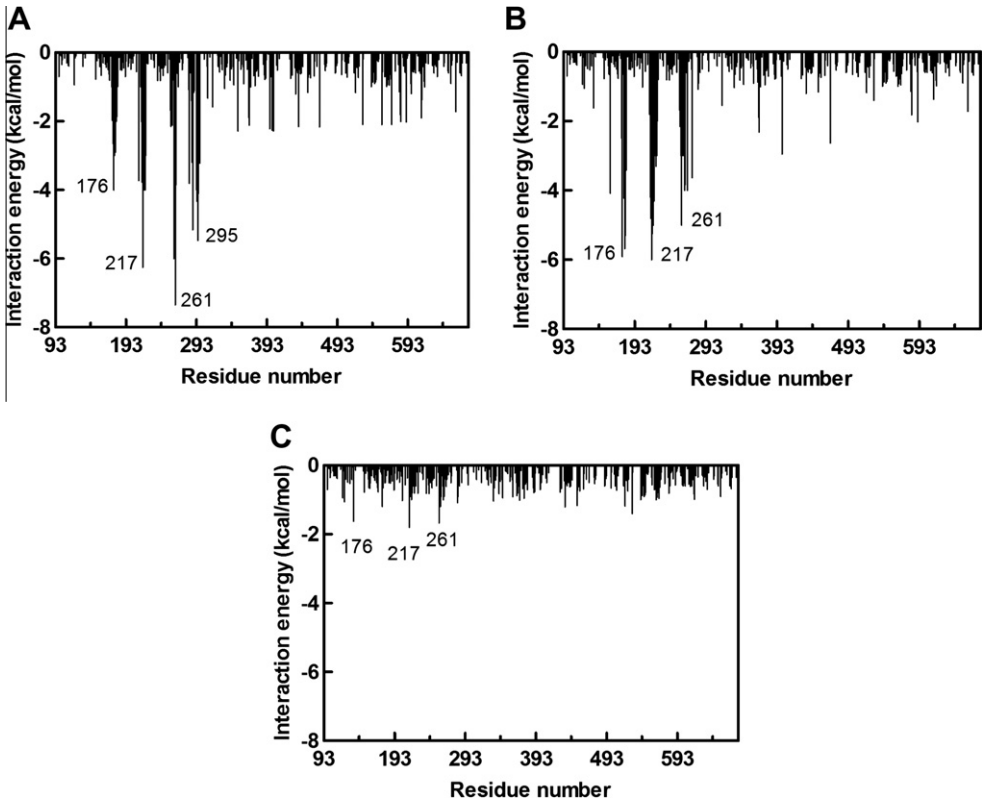

Figure 6. Compound–residue interaction spectrum of BVDV RdRp/**32** (A), BVDV RdRp/**27** (B), and BVDV RdRp/**56** (C) as obtained from the MM/GBSA analysis. The residue BVDV RdRp is reported along the *x*-axis, while the *y*-axis denotes the interaction energy between each inhibitor and the RdRp specific residue.

Table 7
Free energy components and total binding free energies for compounds **32** and **42** on resistant mutant BVDV RdRps

	K131E/E291G **32**	I261M/E291G **42**
ΔE_{VDW}	−48.11 (0.12)	−47.23 (0.15)
ΔE_{EL}	−21.34 (0.22)	−22.19 (0.28)
ΔG_{PB}	53.99 (0.17)	55.23 (0.17)
ΔG_{NP}	−5.18 (0.01)	−5.32 (0.00)
$T\Delta S$solute	14.11 (0.83)	13.30 (0.77)
ΔG_{bind}	***−6.53***	***−6.21***

All values are in kcal/mol. Errors are given in parenthesis as standard errors of the mean.

available experimental information (see Table 3). Also, the major variations in the free energy of binding components in the case of the mutant proteins affect both the van der Waals/hydrophobic and electrostatic contributions to binding, which exhibit a remarkable decrease in both cases. Indeed, by defining these variations as $\Delta\Delta E_{VDW/NP} = \Delta E_{VDW/NP}(\text{mutant}) - \Delta E_{VDW/NP}(\text{wild-type})$ and $\Delta\Delta E_{EL/PB} = \Delta E_{EL/PB}(\text{mutant}) - \Delta E_{EL/PB}(\text{wild-type})$ for each energetic component, respectively, it can be readily seen that a negative value of the quantity $\Delta\Delta E$ will indicate a stabilization of the corresponding interaction, whilst a positive value will signal a decrease in stabilizing interaction upon residue(s) substitution(s). Accordingly, for compound **32** we have $\Delta\Delta E_{VDW/NP}$ = +1.00 kcal/mol and $\Delta\Delta E_{EL/PB}$ = +2.32 kcal/mol, while for compound **42** we have $\Delta\Delta E_{VDW/NP}$ = +2.64 kcal/mol and $\Delta\Delta E_{EL}$ = +0.04 kcal/mol, ultimately resulting in an overall destabilizing contribution of $\Delta\Delta E$ = +3.32 kcal/mol in case of compound **32**, and $\Delta\Delta E$ = +2.68 kcal/mol for compound **42**.

In order to perform a full investigation of the influence of these double mutations on the binding of the enzymes with the respective inhibitors, the compound–residue interaction energy analysis described above for the wild-type case was applied. Figure 7A shows the difference between the ligand–residue interactions of the wild-type RdRp/**32** complex and those of the (K131E/E291G) double mutant RdRp/**32** complex, while Figure 7B illustrates the same quantity in the case of wild-type/(I261M/E291G) double mutant RdRp/**42** complex, respectively. By definition, unfavorable residues in the mutant protein will be characterized by positive values in these figures; vice versa, negative values of the interaction energy difference will highlight favorable residues in mutant protein binding. As shown in Figure 7, other residues in addition to the mutant ones afford a contribution to the loss of binding in the mutated proteins. In the case of compound **32** (see Fig. 7A), the first, unfavorable effect of the presence of the mutant residues is seen to affect those residues clustered around the mutant site K131E, and is mainly due to a long-range conformational change propagation which extends to the portion of the flexible loop involving residues from K255 to D271. The second, unfavorable cluster is located on S176 and is strictly correlated to the third, unfavorable cluster centered on Y289. This evidence points out that, notwithstanding the fact that several wild type strains of BVDV feature an arginine at position 176 instead of the wild-type serine, this residue might play a critical role when coupled to the presence of other mutant amino acids. Also, the overall readjustment of the binding site in the presence of E291G leads to the overall worsening of the interaction energies of residues K131 and S176 upon compound binding. Interestingly, however, the two important residues I261 and K263 gain a little in terms of favorable interaction energy with **32**, always by virtue of the overall rearrangement of the binding site. For compound **42** in the binding pocket of the I261M/E291G double-mutant BVDV RdRp, the unfavorable and favorable residues can be grouped into three clusters. Interestingly, the rearrangement of the binding site in the presence of the mutant residue I261M yields a first, favorable cluster of residues around this

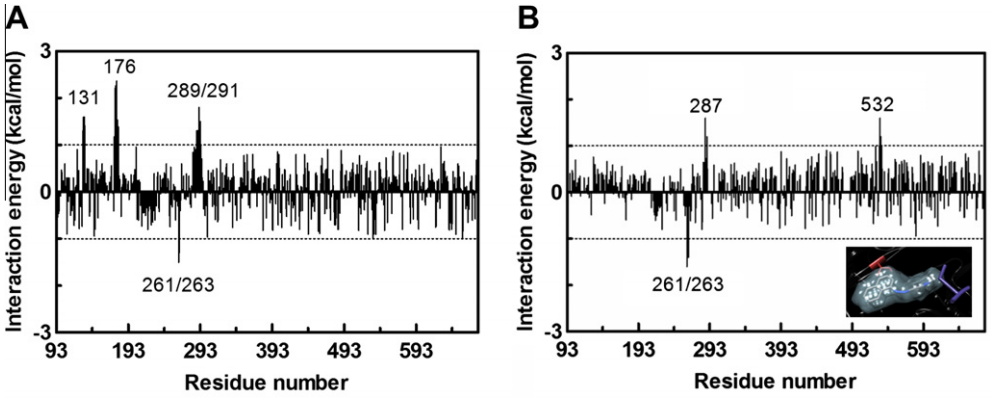

Figure 7. Distribution of the difference between the ligand–residue interactions of (A) the wild-type RdRp/**32** complex and those of the (K313E/E291G) double mutant RdRp/**32** complex, and (B) the same quantity in the case of wild-type/(I261M/E291G) double mutant RdRp/**42** complex, as obtained from the MM/GBSA analysis. Only those residues with absolute difference values larger than 1 kcal/mol are labeled for clarity. The ±1 kcal/mol value cutoff is highlighted by a dotted line. The insert in panel B highlights the steric clashes between **42**, portrayed in atom-colored sticks with its van der Waals surface in light blue, and residues I287 (brown sticks) and S532 (dark slate blue sticks), respectively.

position. On the other hand, the second, unfavorable cluster is centered on I287, as a result of a steric clash of the same residue and the condensed aromatic moiety of the inhibitor, while the third, again unfavorable cluster is mapped around S532, where another sterical repulsion between residues lining the binding cleft and compound **42** is observed (see Fig. 7B).

Lastly, while writing this manuscript, an interesting paper was published on *N*-sulfonylanthranilic acid derivatives as inhibitors of the dengue RdRp.[39] In this work, a computational study was performed to identify the possible compound binding site on the Dengue polymerase. Although further experimental evidence (e.g., resistant mutants) was not provided, the authors hypothesized that their series of compounds could bind to the Dengue RdRp at an allosteric pocket located between the finger and the thumb regions. This pocket is largely coincident with the binding site on the BVDV polymerase proposed in the present work. Also, as illustrated in Figure 8 and as suggested by ongoing analysis (unpublished), not only the RdRp from Dengue but (and perhaps more importantly) also the same enzyme from HCV can bind our arylazoenamine derivatives in the same region with a considerable affinity, in line with the preliminary data reported for HCV in Table 5.

Based on the biological evidences and the modeling results, our series of compounds may destabilize the BVDV replication complex, or a downstream protein–protein interaction required for efficient RNA synthesis, as proposed for other allosteric inhibitors of BVDV RdRp. Indeed, both resistant mutations, I261M and E291G, are located on the same surface of the fingers domain, near the N-terminal domain binding site, which, in turn, is near the entrance of the template binding channel. This surface would provide a good binding site for attachment of other proteins in the replication complex, and possibly modulate binding of the template. As an example, since viral genomic RNA is replicated via a double-stranded RNA intermediate, the helicase could bind on the surface near the template binding channel of the polymerase and unwind the double-stranded RNA to allow only the template strand to enter its binding channel.

As a valid alternative, which could justify also the inhibitory effects observed for compounds **32** and **42** with respect to HCV RdRp (see Table 5), the following mechanism could be considered. In the HCV enzyme, as well as in the corresponding proteins from φ6 and foot-and-mouth disease viruses,[33,40,41] the fingertip region forms an entrance of the template binding channel. In the case of the BVDV, the N-terminal domain is also involved in template binding. A change between an 'open' and a 'closed' conformation involving the fingers and the thumb domains has been suggested as a possible mechanism for translocation of the template. Accordingly, a 'freezing' of the fingertip movement upon inhibitor binding could potentially interfere with enzyme activity. Notably, should the hampering of movement of the fingertip region the molecular mechanisms of RdRp inhibition, it might really constitute an important strategy in selective antiviral drug development, as only viral RdRp feature a fingertip region.

5. Conclusions

In the light of the interesting biological data presented by our series of arylazoenamines as selective and potent inhibitors of BVDV replication,[22] in this work we applied a combined experimental/molecular modeling strategy to study in more detail the interactions between our molecules and the BVDV RNA dependent RNA polymerase.

Accordingly, BVDV mutants resistant to the lead compounds in our series were isolated and the mutant residues on the target RdRp were identified. Cross-resistance studies with other known BVDV RdRp inhibitors were carried out, both to confirm the viral protein target and the role of the mutant residues in conferring drug resistance. The final assessment of the viral polymerase as a molecular target of our compounds was achieved by enzymatic inhibition assays. The two lead compounds **32** and **42** inhibited both BVDV and HCV polymerase, thus confirming the suitability of BVDV as a surrogate model for anti-HCV drug development.

Starting from our published three-dimensional pharmacophore model for the arylazoenamine derivatives as inhibitors of the BVDV RdRp,[22] all active compounds were then docked in a putative binding site on the BVDV RdRp. This step involved a thorough search for a protein binding pocket that could satisfy all the pharmacophore requirements and included the residues found mutated in virus cultures resistant to our molecules. In a further step, molecular dynamics simulations combined with MM/PBSA calculations were performed on the best docking hit for each compound. The calculated free energy of binding between the inhibitors and their target protein showed the same trend of the corresponding experimentally determined EC_{50} values for the entire molecular series. This was an encouraging performance, given that all molecular modeling studies were performed in the absence of any available crystal structure of the protein in complex with an inhibitor. Also, the adopted procedure was able to correctly predict drug binding affinities in the presence of mutated protein residues involved in drug resistance. A deeper insight into the binding energetics and

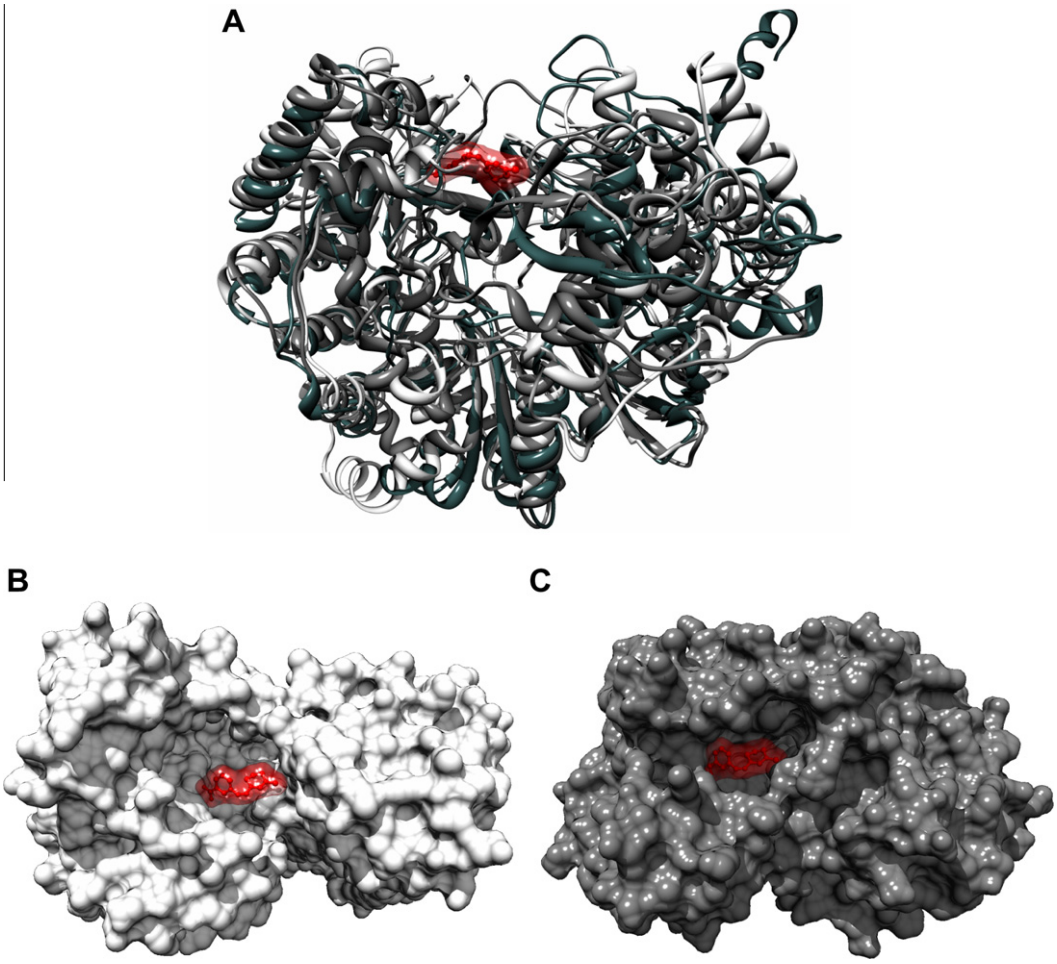

Figure 8. (A) Superposition of the three-dimensional structure of RdRP from BVDV (dark gray), Dengue (white), and HCV (light gray) with compound **32** docked in the putative binding region between the finger and the thumb domains of the enzyme. Detailed space filling representation of the (B) Dengue RdRp and (C) HCV RdRP molecular surfaces and compound **32** docked into the protein putative binding site. In all panels, the inhibitor is represented as red sticks-and-balls with its van der Waals surface highlighted in red as well.

mechanism of our compound series was obtained by splitting the total free energy of binding into contributions from individual ligand–residue pairs. This approach led us to the discovery that other residues in addition to the mutated ones are related to the loss of binding and that, as discussed for instance in the case of compound **32**, the presence of the double mutation K131E/E291G results in an overall distortion of the binding site and a general weakening of the favorable interactions relatively to the wild-type protein binding site. In other words, the conformational change of the active site induced by the presence of the double mutation and the inability of the ligand to adapt to the 'distorted' binding site could explain the observed drug resistance against our arylazoenamine derivatives.

6. Materials and methods

6.1. Cell-based assays

6.1.1. Compounds

All compounds were dissolved in DMSO at 100 mM and then diluted in culture medium.

6.1.2. Cell lines and viruses

Cell lines and viruses were purchased from American Type Culture Collection (ATCC). The absence of mycoplasma contamination was checked periodically by the Hoechst staining method. Cell lines supporting the multiplication of bovine viral diarrhea virus (BVDV), strain NADL (ATCC VR-534), were the Madin Darby Bovine Kidney (MDBK).

6.1.3. Cytotoxicity assays

For cytotoxicity tests, run in parallel with antiviral assays, MDBK cells were resuspended in 96 multiwell plates at an initial density of 6×10^5 cells/mL, in maintenance medium, without or with serial dilutions of test compounds. Cell viability was determined after 48–96 h at 37 °C in a humidified CO_2 (5%) atmosphere by the MTT method.[42]

6.1.4. Antiviral assays

Compounds activity against BVDV was based on inhibition of virus-induced cytopathogenicity in MDBK cells acutely infected with a m.o.i. of 0.01. Briefly, MDBK cells were seeded in 96-well plates at a density of 3×10^4 cells/well and were allowed to form confluent monolayers by incubating overnight in growth medium at 37 °C in a humidified CO_2 (5%) atmosphere. Cell monolayers were then infected with 50 μL of a proper virus dilution in maintenance medium (MEM-E with L-glutamine, supplemented with 0.5% inactivated FBS and 1 mM sodium pyruvate, 1% kanamycin) to give an m.o.i of 0.01. After 1 h, 50 μL of maintenance medium, without or with serial dilutions of test compounds, were added. After a

3–4-day incubation at 37 °C, cell viability was determined by the MTT method. NM 108 (2′-β-methyl-guanosine) was used as reference compound.

6.1.5. Selection of drug-resistant mutants

Drug resistant variants were selected by serial passages of viruses in the presence of stepwise doubling drug concentrations, starting from a cell culture infected with an m.o.i. of 0.01, and treated with a drug concentration equal to the EC_{50}. Usually, the amount of virus obtained after each passage was sufficient to determine infection of the next cell culture which, after infection and washing, was incubated with a double amount of the selecting drug. Resistant virus preparations were subjected to RNA extraction, RT-PCR and genome sequencing to identify the mutation patterns responsible for resistance.

6.1.6. Molecular analysis of resistant viruses

Viral RNAs from wild-type and drug resistant mutants were obtained using the QIAamp viral RNA minikit (QIAGEN), starting from 140 μL of cell-free viral suspensions containing about 10^6 PFU/mL, in order to determine the nucleotide sequence of the NS3 and NS5B genes of BVDV genome. Reverse transcription reactions were carried out using the Superscript II enzyme (INVITROGEN) and PCR reactions using the *Pfx* Platinum enzyme (INVITROGEN), following the manufacturer's protocol. Primers used in reverse transcription were RT3 5′-CCCCACAAACCATATCT GATTATTTCTTCTTTA-3′ and RT5b 5′-GTAGATAATCTTGACTACTG TTTAGCTCTTGAG-3′, that respectively bind 360 bp downstream the NS3 gene and 90 bp downstream the NS5b gene.

The nonstructural region containing NS3 gene was amplified by a PCR reaction, carried out with primers A (5′-TAAAAATGCT CATGGTAGGCAACCT-3′) and B (5′-TTATCATTGGGACATGCCTCTTT GA-3′), resulting in a PCR fragment of 2205 bp; PCR amplification consisted of: initial denaturation of 3 min; 34 cycles of denaturation at 94 °C for 30 s, annealing at 56 °C for 30 s and extension at 68 °C for 2.5 min; final extension at 68 °C for 5 min. The nonstructural region containing NS5B gene was amplified by two different PCR reactions, carried out respectively with primers C (ATTATAAAGGAGGTAGGCTCAAGGA) and D (CCATCTGCTGTTAT AACTGGTACTT) and with primers E (5′-ACCCCCTTGTTCAA- CA TCTTTGATA-3′) and F (5′-GTGGACGGTCCCAACTATATTTATA-3′), resulting into two PCR fragments of 1223 bp and 1792 bp. PCR amplification consisted of: initial denaturation of 3 min; 34 cycles of denaturation at 94 °C for 30 s, annealing at 52.5 °C for 30 s and extension at 68 °C for 2 min; final extension at 68 °C for 5 min.

PCR fragments were purified using the QIAquick PCR Purification kit (QIAGEN) and analyzed using the cycle-sequencing method (CIBIACI service of University of Firenze). Both DNA strands were sequenced with specific primers. The comparative analysis of the chromatograms allowed us to deduce the mutation patterns responsible for resistance to compound.

6.1.7. Expression of BVDV-NS5BΔ24 polymerase

Expression and purification of BVDV-NS5BΔ24 polymerase have been done as previously described.[2] Briefly, the expression plasmid encoding the N terminal His-tagged C terminal 24-amino-acid-deleted BVDV-NS5B was transformed into the *Escherichia coli* strain Rosetta™ 2 (DE3) pLysS (Novagene), and the transformants were then cultured in 5 ml of LB medium with 25 μg/ml Kanamycin and 30 μg/ml chloramphenicol at 30 °C overnight. Cultures were diluted into 1 l of LB medium with 25 μg/ml Kanamicin and 30 μg/ml chloramphenicol and incubated at 30 °C until the A_{600} reached 0.6–0.7. These cultures were then induced overnight with 1 mM isopropyl-β-D-thiogalactopyranoside. The cells were harvested by centrifugation and stored at −80 °C until the purification.

6.1.8. Expression of HCV1b-NS5BΔ21 polymerase

The gene coding for the C-terminal 21-amino-acid-deleted NS5B polymerase (NS5BΔ21) of HCV BK strain (genotype 1b) C-terminally fused with a 6xHis-tag was cloned between the *Bam*HI and *Xho*I cloning sites of the pET-21a(+) expression plasmid (Novagen). The construct encoding the 6xHis-tagged HCV1b-NS5BΔ21 protein under the control of the T7 RNA polymerase promoter was confirmed by dideoxynucleotide sequencing and transformed into the *Escherichia coli* strain Rosetta™ 2(DE3)pLysS (Novagene). A single colony expressing the 6xHis-tagged HCV1b-NS5BΔ21 protein was selected and cultured in 5 mL of LB medium supplemented with 100 μg/mL ampicillin and 30 μg/mL chloramphenicol at 30 °C overnight. The culture was diluted into 1 L of the same culture medium and incubated at 30 °C until the absorbance reached 0.6–0.7 at 600 nm. The culture was then induced overnight at 25 °C with 1 mM isopropyl-β-D-thiogalactopyranoside. The cells were harvested by centrifugation and stored at −80 °C until the purification.

6.1.9. In vitro RNA-dependent RNA polymerase activity assays

In vitro synthesis assays were performed in 96-well plates using 10 μg/mL poly(rC) (GE Healthcare, formerly Amersham Biosciences) as template and 0.1 μg/mL oligo $(rG)_{12}$ (Invitrogen) as primer and 80 μM GTP (Invitrogen) as substrate in a 20 μL reaction mixture containing 20 mM Tris/HCl pH 7.0, 1 mM dithiothreitol, 25 mM NaCl, 20 U/mL RNasin (Promega), 0.5 mM $MnCl_2$ or 5 mM $MgCl_2$, 5% DMSO, 5% glycerol and 500–600 ng of each purified protein. After an enzyme/drug pre-incubation for 30 min at room temperature, reactions were started by the addition of GTP. 1 μL of threefold serial dilutions of test compounds, or DMSO alone (as a negative control of inhibition), or the nucleotide analogue 3′-deoxyguanosine-5′-triphosphate (3′-dGTP) (tebu-bio) (as a positive control of inhibition), was added to the reactions and incubated for 120 min at 37 °C (for BVDV-NS5BΔ24) or 25 °C (for HCV1b-NS5BΔ21), then stopped by the addition of 2 μL of 200 mM EDTA. 138 μL of PicoGreen Quantitation Reagent (Molecular Probes), diluted 1/345 in TE, were added into each sample and incubated for 5 min at room temperature protected from light. After an excitation at ~480 nm, the fluorescence was measured at ~520 nm in a fluorescence microplate reader (VICTOR[3] Multilabel Plate Reader, PerkinElmer). 'Relative fluorescence' was calculated by subtracting the mean fluorescence of the blank from all samples and converted into percent of activity. Percent of residual activity was then plotted versus the compound concentrations. Dose–response curves were fit with Kaleidagraph (Synergy Software) to obtain the drug concentration that provides 50% of inhibition (IC_{50}).

6.1.10. HCV replicon assays

Huh-7 cells containing HCV Con1 subgenomic replicon (GS4.1 cells), kindly provided by C Seeger (Fox Chase University, Philadelphia, PA, USA), were grown in DMEM supplemented with 10% foetal bovine serum (FBS), 2 mM L-glutamine, 110 mg/L sodium pyruvate, 0.1 mM non-essential amino acids, 100 U/mL penicillin–streptomycin and 0.5 mg/mL G418 (Invitrogen Corp, Carlsbad, CA, USA). For dose–response testing, the cells were seeded in 96-well plates at 7.5×10^3 cells/well in a volume of 50 μL of 10 twofold serial dilutions of compounds (highest concentration, 75 μM) were added and cell cultures were incubated at at 37 °C/5% CO_2 in the presence of 0.5% DMSO. Alternatively, compounds were tested at a single concentration of 15 μM. In all cases, Huh-7 cells lacking the HCV replicon served as a negative control. The cells were incubated in the presence of compounds for 72 h after which they were monitored for expression of the NS4A protein by ELISA. For this, the plates were then fixed for 1 min with 1:1 acetone–methanol, washed twice with PBS containing 0.1% Tween 20, blocked for 1 h at room temperature with TNE buffer containing 10% FBS and then incubated for 2 h at 37 °C with the anti-NS4A

mouse monoclonal antibody A-236 (ViroGen, Watertown, MA, USA) diluted in the same buffer. After washing three times with PBS containing 0.1% Tween 20, the cells were incubated for 1 h at 37 °C with anti-mouse immunoglobulin G–peroxidase conjugate in TNE buffer with 10% FBS. After washing as described above, the reaction was developed with *o*-phenylenediamine (Zymed, San Francisco, CA, USA). The reaction was stopped after 30 min with 2 N H_2SO_4 and the absorbance was read at 492 nm using Sunrise Tecan (Durham, NC, USA) Spectrophotometer. EC_{50} values were determined from the % inhibition versus concentration data using a sigmoidal non-linear regression analysis based on four parameters with Tecan Magellan software. When screening at a single concentration, the results were expressed as % inhibition at 15 μM. For cytotoxicity evaluation, GS4.1 were treated with compounds as described above and cellular viability was monitored using the Cell Titer 96 Aqueous one solution cell proliferation assay (Promega Corp, Madison, WI, USA). CC_{50} values were determined from the % cytotoxicity versus concentration data with Tecan Magellan software as described above.

6.2. Molecular modeling

The entire computational recipe (see Supplementary data) involved the following program packages: AutoDock (v. 4.0),[43] AMBER 9.0,[44] Materials Studio (v.4.3),[45] InsightII (v.2001),[46] and in-house developed codes (stand-alone and add-on to the commercial software). Molecular graphics images were produced using the UCSF Chimera package (v.1.4).[47] All high-resolution figures were obtained by processing Chimera files with POV-Ray (v.3.6).[48] The extensive, parallel molecular dynamics analyses were performed using 64 processors of the Tartaglia cluster at the University of Trieste (Trieste, Italy), as well as the same number of processors on the IBM/BCX cluster at the CINECA supercomputer center (Bologna, Italy).

The optimized structure of the RNA-dependent RNA polymerase (RdRp) of BVDV were taken from our previous work.[22] The putative binding site for our compounds on the BVDV RdRp was determined using the *ActiveSite_Search* option of the *Binding Site* module of InsightII.[46]

The optimized structures of the inhibitors were docked into the BVDV polymerase allosteric binding site by applying a consolidated procedure[22,31,32,37,38] based on AutoDock 4.0.[43] Following the docking procedure, the structure of all compounds was subjected to cluster analysis with a tolerance of 1 Å for an all-atom root-mean-square (RMS) deviation from a lower-energy structure representing each cluster family. In the absence of any relevant crystallographic information, the structure of each resulting complex characterized by the lowest interaction energy in the prevailing cluster was selected for further evaluation.

Each best substrate/RdRp complex, resulting from the automated docking procedure, was allowed to relax in a 55-Å radius sphere of TIP3P water molecules.[49] The resulting system was minimized with a gradual decrease in the position restraints of the protein atoms. At the end of the relaxation process, all water molecules beyond the first hydration shell (i.e., at a distance >3.5 Å from any protein atom) were removed. Finally, to achieve electroneutrality, a suitable number of counterions were added, in the positions of the largest electrostatic potential, as determined by the *Leap* module within Amber 9.0. Each system was gradually heated to 310 K at three intervals, allowing a 500 ps interval per each 100 K, and then equilibrated for 2 ns at 310 K, followed by 2 ns of data collection runs, necessary for the estimation of the free energy of binding (vide infra).

The binding free energy ΔG_{bind} of each RdRp/drug complex in water was calculated according to the procedure termed Molecular Mechanic/Poisson–Boltzmann Surface Area (MM/PBSA), and originally proposed by Srinivasan et al.[35] All energetic analyses were performed for a single 5 ns MD trajectory of RdRp/inhibitor complex considered, with 500 unbound protein and drug snapshots taken from the frames in the equilibrated data production phase of that trajectory. The binding free energy for each ligand/receptor system, ΔG_{bind}, was obtained as:

$$\Delta G_{bind} = \Delta H_{bind} - T\Delta S_{bind} \quad (1)$$

$$\Delta H_{bind} = \Delta E_{MM} + \Delta G_{solv} \quad (2)$$

The average values of the enthalpic contribution to ΔG_{bind} were calculated by summing the molecular mechanics energies ($\Delta E_{MM} = \Delta E_{EL} + \Delta E_{VDW}$) and the solvation free energies ($\Delta G_{solv} = \Delta G_{PB} + \Delta G_{NP}$). The polar component of ΔG_{sol} was evaluated using the Poisson–Boltzmann (PB) approach,[50] while the non-polar contribution to the solvation energy was calculated as $\Delta G_{NP} = \gamma(SASA) + \beta$, in which $\gamma = 0.00542$ kcal/Å^2, $\beta = 0.92$ kcal/mol, and SASA is the solvent-accessible surface estimated with the MSMS program.[51] Finally, the last parameter in Eq. 1, that is, the change in solute entropy upon association $-T\Delta S_{bind}$, was calculated through normal-mode analysis.

Acknowledgments

Financial support from Italian MIUR (FIRB RBNE01J3SK01) is gratefully acknowledged.

Supplementary data

Supplementary data associated with this article can be found, in the online version, at doi:10.1016/j.bmc.2010.06.065.

References and notes

1. Monath, T. P. *Bull. Soc. Pathol. Exot.* **2006**, *99*, 341.
2. Hayashi, P. H.; Di Bisceglie, A. M. *Med. Clin. North Am.* **2005**, *89*, 371.
3. WHO. Global surveillance and control of hepatitis *J. Viral Hepat.* **1999**, *6*, 35.
4. Memon, M. I.; Memon, M. A. *J. Viral Hepat.* **2002**, *9*, 84.
5. Echevarria-Mayo, J. M. *Enferm. Infect. Microbiol Clin.* **2006**, *24*, 4.
6. Bosch, F. X.; Ribes, J.; Cleries, R.; Diaz, M. *Clin. Liver Dis.* **2005**, *9*, 191.
7. Fried, M. W.; Shiffman, M. L.; Reddy, K. R.; Smith, C.; Marinos, G.; Gonçales, F. L., Jr.; Häussinger, D.; Diago, M.; Carosi, G.; Dhumeax, D.; Craxi, A.; Lin, A.; Hoffman, J.; Yu, J. *N. Eng. J. Med.* **2002**, *347*, 975.
8. Pearlman, B. L. *Am. J. Med.* **2004**, *117*, 344.
9. Huang, Z.; Murray, M. G.; Secrist, J. A., III *Antiviral Res.* **2006**, *71*, 351.
10. Lindberg, A. L. *Vet. Q.* **2003**, *25*, 1–16.
11. O'Connor, A. M.; Sorden, S. D.; Apley, M. D. *Am. J. Vet. Res.* **2005**, *66*, 2130.
12. Chase, C. C.; Elmowalid, G.; Yousif, A. A. *Vet. Clin. North Am. Food Anim. Pract.* **2004**, *20*, 95.
13. Houe, H. *Biologicals* **2003**, *31*, 137.
14. Greiser-Wilke, I.; Grummer, B.; Moenning, W. *Biologicals* **2003**, *31*, 113.
15. Buckwold, V. E.; Beer, B. E.; Donis, R. O. *Antivir. Res.* **2003**, *60*, 1.
16. Pietschmann, T.; Bartenschlager, R. *Curr. Opin. Drug Disc. Dev.* **2001**, *4*, 657.
17. (a) Lindenbach, B. D.; Evans, M. J.; Syder, A. J.; Wolk, B.; Tellinghuisen, T. L.; Liu, C. C.; Maruyama, T.; Hynes, R. O.; Burton, D. R.; McKeating, J. A.; Rice, C. M. *Science* **2005**, *309*, 623; (b) Wakita, T.; Pietschmann, T.; Kato, T.; Date, T.; Miyamoto, M.; Zhao, Z.; Murthy, K.; Habermann, A.; Krausslich, H. G.; Mizokami, M.; Bartenschlager, R.; Liang, T. J. *Nat. Med.* **2005**, *11*, 791; (c) Zhong, J.; Gastaminza, P.; Cheng, G.; Kapadia, S.; Kato, T.; Burton, D. R.; Wieland, S. F.; Uprichard, S. L.; Wakita, T.; Chisari, F. V. *Proc. Natl. Acad. Sci. U.S.A.* **2005**, *102*, 9294.
18. (a) Sun, J.-H.; Lemm, J. A.; O'Boyle, D. R., II; Racela, J.; Colonno, R.; Gao, M. *J. Virol.* **2003**, *77*, 6753; (b) Paeshuyse, J.; Leyssen, P.; Mabery, E.; Boddeker, N.; Vrancken, R.; Froeyen, M.; Ansari, I. H.; Dutartre, H.; Rozenski, J.; Gil, L. H. V. G.; Letellier, C.; Lanford, R.; Canard, B.; Koenen, F.; Kerkhofs, P.; Donis, R. O.; Herdewijn, P.; Watson, J.; De Clercq, E.; Puerstinger, G.; Neyts, J. *J. Virol.* **2006**, *80*, 149–160; (c) Puerstinger, G.; Paeshuyse, J.; Herdewijn, P.; Rozenski, J.; De Clercq, E.; Neyts, J. *Bioorg. Med. Chem. Lett.* **2006**, *16*, 5345; (d) Tabarrini, O.; Manfroni, G.; Fravolini, A.; Cecchetti, V.; Sabatini, S.; De Clercq, E.; Rozenski, J.; Canard, B.; Dutartre, H.; Paeshuyse, J.; Neyts, J. *J. Med. Chem.* **2006**, *49*, 2621; (e) Puerstinger, G.; Paeshuyse, J.; Heinrich, S.; Mohr, J.; Schraffl, N.; De Clercq, E.; Neyts, J. *Bioorg. Med. Chem. Lett.* **2007**, *17*, 5111; (f) Paeshuyse, J.; Chezal, J.-M.; Froeyen, M.; Leyssen, P.; Dutartre, H.; Vrancken, R.; Canard, B.; Letellier, C.; Li, T.; Mittendorfer, H.; Koenen, F.; Kerkhofs, P.; De Clercq, E.; Herdewijn, P.; Puerstinger, G.; Gueiffier, A.; Chavignon, O.; Teulade, J.-C.; Neyts, J. *J. Virol.* **2007**, *81*, 11046; (g) Sako, K.; Aoyama, H.; Sato, S.; Hashimoto, Y.; Baba, M.

Bioorg. Med. Chem. **2008**, *16*, 3780; (h) Hosoda, S.; Aoyama, H.; Goto, Y.; Salim, M. T. A.; Okamoto, M.; Hashimoto, M.; Baba, M.; Hashimoto, Y. *Bioorg. Med. Chem. Lett.* **2009**, *19*, 3157.
19. Gong, Y.; Trowbridge, R.; Macnaughton, T. B.; Westaway, E. G.; Shannon, A. D.; Gowans, E. J. *J. Gen. Virol.* **1996**, *77*, 2729.
20. Nuttall, P. A. *Arch. Virol.* **1980**, *66*, 365.
21. Leyssen, P.; De Clercq, E.; Neyts, J. *Clin. Microbiol. Rev.* **2000**, *13*, 67.
22. Tonelli, M.; Boido, V.; Canu, C.; Sparatore, A.; Sparatore, F.; Paneni, M. S.; Fermeglia, M.; Pricl, S.; La Colla, P.; Casula, L.; Ibba, C.; Collu, D.; Loddo, R. *Bioorg. Med. Chem.* **2008**, *16*, 8447.
23. Baginski, S. G.; Pevear, D. C.; Seipel, M.; Sun, S. C. C.; Benetatos, C. A.; Chunduru, S. K.; Rice, C. M.; Collett, M. S. *Proc. Natl. Acad. Sci. U.S.A.* **2000**, *97*, 7981.
24. Migliaccio, G.; Tomassini, J. E.; Carroll, S. S.; Tomei, L.; Altamura, S.; Bhat, B.; Bartholomew, L.; Bosserman, M. R.; Ceccacci, A.; Colwell, L. F.; Cortese, R.; De Francesco, R.; Eldrup, A. B.; Getty, K. L.; Hou, X. S.; LaFemina, R. L.; Ludmerer, S. W.; MacCoss, M.; McMasters, D. R.; Stahlhut, M. W.; Olsen, D. B.; Hazuda, D. J.; Flores, O. A. *J. Biol. Chem.* **2003**, *278*, 49164.
25. King, R. W.; Scarnati, H. T.; Priestley, E. S.; De Lucca, I.; Bansal, A.; Williams, J. K. *Antiviral Chem. Chemother.* **2002**, *13*, 315.
26. Tonelli, M.; Boido, V.; La Colla, P.; Loddo, R.; Posocco, P.; Paneni, M. S.; Fermeglia, M.; Pricl, S. *Bioorg. Med. Chem.* **2010**, *18*, 2304.
27. (a) Lai, V. C.; Kao, C. C.; Ferrari, E.; Park, J.; Uss, A. S.; Wright-Minogue, J.; Hong, Z.; Lau, J. Y. *J. Virol.* **1999**, *73*, 10129; (b) Dimitrova, M.; Imbert, I.; Kieny, M. P.; Schuster, C. *J. Virol.* **2003**, *77*, 5401; (c) Piccininni, S.; Varaklioti, A.; Nardelli, M.; Dave, B.; Raney, K. D.; McCarthy, J. E. *J. Biol. Chem.* **2002**, *277*, 45670.
28. Angusti, A.; Manfredini, S.; Durini, E.; Ciliberti, N.; Vertuani, S.; Solaroli, N.; Pricl, S.; Ferrone, M.; Fermeglia, M.; Loddo, R.; Secci, B.; Visioli, A.; Sanna, T.; Collu, G.; Pezzullo, M.; La Colla, P. *Chem. Pharm. Bull.* **2008**, *56*, 423.
29. Choi, K. H.; Groarke, J. M.; Young, D. C.; Kuhn, R. J.; Smith, J. L.; Pevear, D. C.; Rossmann, M. G. *Proc. Natl. Acad. Sci. U.S.A.* **2004**, *101*, 4425.
30. Choi, K. H.; Gallei, A.; Becher, P.; Rossmann, M. G. *Structure* **2006**, *14*, 1107.
31. Tonelli, M.; Vazzana, I.; Tasso, B.; Boido, V.; Sparatore, F.; Fermeglia, M.; Paneni, M. S.; Posocco, P.; Pricl, S.; La Colla, P.; Ibba, C.; Secci, B.; Collu, G.; Loddo, R. *Bioorg. Med. Chem.* **2009**, *17*, 4425.
32. Carta, A.; Loriga, M.; Paglietti, G.; Ferrone, M.; Fermeglia, M.; Pricl, S.; Sanna, T.; Ibba, C.; La Colla, P.; Loddo, R. *Bioorg. Med. Chem.* **2007**, *15*, 1914.
33. O'Farrell, D.; Trowbridge, R.; Rowlands, D.; Jäger, J. *J. Mol. Biol.* **2003**, *326*, 1025.
34. Kim, Y.-C.; Russell, W. K.; Ranjith-Kumar, C. T.; Thomson, M.; Russell, D. H.; Kao, C. C. *J. Biol. Chem.* **2005**, *280*, 38011.
35. Srinivasan, J.; Cheatham, T. E.; Cieplak, P.; Kollman, P. A.; Case, D. A. *J. Am. Chem. Soc.* **1998**, *120*, 9401.
36. Kalra, P.; Reddy, V.; Jayaram, B. *J. Med. Chem.* **2001**, *44*, 4325–4338.
37. For recent applications of our MDSA protocol see, for instance: (a) Zampieri, D.; Mamolo, M. G.; Laurini, E.; Fermeglia, M.; Posocco, P.; Pricl, S.; Banfi, E.; Scialino, G.; Vio, L. *Bioorg. Med. Chem.* **2009**, *17*, 4693; (b) Mazzei, M.; Nieddu, E.; Miele, M.; Balbi, A.; Ferrone, M.; Fermeglia, M.; Mazzei, M. T.; Pricl, S.; La Colla, P.; Marongiu, F.; Ibba, C.; Loddo, R. *Bioorg. Med. Chem.* **2008**, *16*, 2591; (c) Zampieri, D.; Mamolo, M. G.; Vio, L.; Banfi, E.; Scialino, G.; Fermeglia, M.; Ferrone, M.; Pricl, S. *Bioorg. Med. Chem.* **2007**, *15*, 7444; (d) Carta, A.; Loriga, M.; Piras, S.; Paglietti, G.; Ferrone, M.; Fermeglia, M.; Pricl, S.; La Colla, P.; Collu, G.; Sanna, T.; Loddo, R. *Med. Chem.* **2007**, *3*, 520. and references cited therein.
38. For a further list of recent applications of the MM/PBSA methodology from our group see, for instance: (a) Pavan, G. M.; Danani, A.; Pricl, S.; Smith, D. K. *J. Am. Chem. Soc.* **2009**, *131*, 9686; (b) Conca, E.; Negri, T.; Gronchi, A.; Fumagalli, E.; Tamborini, E.; Pavan, G. M.; Fermeglia, M.; Pierotti, M. A.; Pricl, S.; Pilotti, S. *Mol. Cancer Ther.* **2009**, *8*, 2491; (c) Woodman, S. E.; Trent, J. C.; Stemke-Hale, K.; Lazar, A. J.; Pricl, S.; Pavan, G. M.; Fermeglia, M.; Gopal, Y. N.; Yang, D.; Podoloff, D. A.; Ivan, D.; Kim, K. B.; Papadopoulos, N.; Hwu, P.; Mills, G. B.; Davies, M. A. *Mol. Cancer Ther.* **2009**, *8*, 2079; (d) McAuliffe, J. C.; Wang, W. L.; Pavan, G. M.; Pricl, S.; Yang, D.; Chen, S. S.; Lazar, A. J.; Pollock, R. E.; Trent, J. C. *Mol. Oncol.* **2008**, *2*, 161; (e) Negri, T.; Pavan, G. M.; Virdis, E.; Greco, A.; Fermeglia, M.; Sandri, M.; Pricl, S.; Pierotti, M. A.; Pilotti, S.; Tamborini, E. *J. Natl. Cancer Inst.* **2009**, *101*, 194; (f) Ferrone, M.; Perrone, F.; Tamborini, E.; Paneni, M. S.; Fermeglia, M.; Suardi, S.; Pastore, E.; Delia, D.; Pierotti, M. A.; Pricl, S.; Pilotti, S. *Mol. Cancer Ther.* **2006**, *5*, 1467; (g) Tamborini, E.; Pricl, S.; Negri, T.; Lagonigro, M. S.; Miselli, F.; Greco, A.; Gronchi, A.; Casali, P. G.; Ferrone, M.; Fermeglia, M.; Carbone, A.; Pierotti, M. A.; Pilotti, S. *Oncogene* **2006**, *25*, 6140; (h) Pricl, S.; Fermeglia, M.; Ferrone, M.; Tamborini, E. *Mol. Cancer Ther.* **2005**, *4*, 1167; (i) Mamolo, M. G.; Zampieri, D.; Vio, L.; Fermeglia, M.; Ferrone, M.; Pricl, S.; Scialino, G.; Banfi, E. *Bioorg. Med. Chem.* **2005**, *13*, 3797.
39. Yin, Z.; Chen, Y. L.; Kondreddi, R. R.; Chan, W. L.; Wang, G.; Ng, R. H.; Lim, J. Y.; Lee, W. Y.; Jeyaraj, D. A.; Niyomrattanakit, P.; Wen, D.; Chao, A.; Glickman, J. F.; Voshol, H.; Mueller, D.; Spanka, C.; Dressler, S.; Nilar, S.; Vasudevan, S. G.; Shi, P. Y.; Keller, T. H. *J. Med. Chem.* **2009**, *52*, 7934.
40. Butcher, S. J.; Grimes, J. M.; Makeyev, E. V.; Bamford, D. H.; Stuart, D. I. *Nature* **2001**, *410*, 235.
41. Ferrer-Orta, C.; Arias, A.; Perez-Luque, R.; Escarmis, C.; Domingo, E.; Verdaguer, V. *J. Biol. Chem.* **2004**, *279*, 47212.
42. Pauwels, R.; Balzarini, J.; Baba, M.; Snoeck, R.; Schols, D.; Herdewijn, P.; Desmyter, J.; De Clercq, E. *J. Virol. Methods* **1988**, *20*, 309.
43. Huey, R.; Morris, G. M.; Olson, A. J.; Goodsell, D. S. *J. Comput. Chem.* **2007**, *28*, 1145.
44. Case, D. A.; Darden, T. A.; Cheatham, T. E., III; Simmerling, C. L.; Wang, J.; Duke, R. E.; Luo, R.; Merz, K. M.; Pearlman, D. A.; Crowley, M.; Walker, R. C.; Zhang, W.; Wang, B.; Hayik, S.; Roitberg, A.; Seabra, G.; Wong, K. F.; Paesani, F.; Wu, X.; Brozell, S.; Tsui, V.; Gohlke, H.; Yang, L.; Tan, C.; Mongan, J.; Hornak, V.; Cui, G.; Beroza, P.; Mathews, D. H.; Schafmeister, C.; Ross, W. S.; Kollman, P. A. *AMBER 9*, University of California, San Francisco, CA USA, 2006.
45. Materials Studio (v.4.3), Accelrys Inc., San Diego (CA), USA.
46. InsightII (v.2001), Accelrys Inc., San Diego (CA), USA.
47. (a) Chimera (v.1.4), Resource for Biocomputing, Visualization, and Informatics at the University of California, San Francisco (CA), USA; (b) Pettersen, E. F.; Goddard, T. D.; Huang, C. C.; Couch, G. S.; Greenblatt, D. M.; Meng, E. C.; Ferrin, T. E. *J. Comput. Chem.* **2004**, *25*, 1605.
48. POV-Ray: Persistence of Vision Raytracer (v. 3.6), Persistence of Vision Pty. Ltd, Williamstown, Victoria, Australia.
49. Jorgensen, W. L.; Chandrasekhar, J.; Madura, J. D.; Impey, R. W.; Klein, M. L. *J. Chem. Phys.* **1983**, *79*, 926.
50. Sitkoff, D.; Sharp, K. A.; Honig, B. *J. Phys. Chem.* **1994**, *98*, 1978.
51. Sanner, M. F.; Olson, A. J.; Spehner, J. C. *Biopolymers* **1996**, *38*, 305.